

Reactive solute transport in physically and chemically heterogeneous porous media with multimodal reactive mineral facies: The Lagrangian approach

Mohamad Reza Soltanian^{1,*}, Robert Ritzl¹, Zhenxue Dai², Chaocheng Huang³

¹Department of Earth and Environmental Sciences, Wright State University, Dayton, OH, 45435

²EES-16, Earth and Environmental Sciences Division, Los Alamos National Laboratory, Mailstop T003, Los Alamos, NM 87545

³Department of Mathematics and Statistics, Wright State University, Dayton, OH, 45435

*Corresponding author. Phone: (937) 775-2201, e-mail: m.rezasoltanian@gmail.com

Abstract

Physical and chemical heterogeneities have a large impact on reactive transport in porous media. Examples of heterogeneous attributes affecting reactive mass transport are the hydraulic conductivity (K), and the equilibrium sorption distribution coefficient (K_d). This paper uses the Deng et al. (2013) conceptual model for multimodal reactive mineral facies and a Lagrangian-based stochastic theory in order to analyze the reactive solute dispersion in three-dimensional anisotropic heterogeneous porous media with hierarchical organization of reactive minerals. An example based on real field data is used to illustrate the time evolution trends of reactive solute dispersion. The results show that the correlation between the hydraulic conductivity and the equilibrium sorption distribution coefficient does have a significant effect on reactive solute dispersion. The anisotropy ratio does not have a significant effect on reactive solute dispersion.

Furthermore, through a sensitivity analysis we investigate the impact of changing the mean, variance, and integral scale of K and K_d on reactive solute dispersion.

Introduction

Reactive transport in porous formations is controlled by heterogeneity in physical and chemical properties (Dagan, 1989; Bellin et al., 1993; Miralles-Wilhelm and Gelhar, 1996; Brusseau and Srivastava, 1997; Rajaram, 1997; Dai et al., 2009; Deng et al., 2010; Soltanian et al., 2014). Examples of these properties are hydraulic conductivity (K), and the equilibrium sorption distribution coefficient (K_d). It has been shown that these parameters are scale-dependent (Allen-King et al., 1998, 2006; Davis et al., 2004; Ritzi et al., 2004; Dai et al., 2007; Ramanathan et al., 2010; Zhang et al., 2013; Ritzi et al., 2013). The spatial variations of physical and chemical heterogeneity are known to be responsible for the scale-dependence of transport parameters such as the retardation factor and the macrodispersivity (Dai et al., 2009; Deng et al., 2013).

Different methods have been proposed for dealing with scale-dependent transport parameters. For example, it is common to use the upscaling process in order to incorporate the effect of small-scale variability on solute transport (Rubin, 2003). Various schemes have been suggested in the literature to upscale reactive transport parameters, as reviewed by Dentz et al. (2011). These include volume averaging (e.g., Whitaker, 1999), stochastic averaging (e.g., Gelhar and Axness, 1983; Dagan, 1984), homogenization (e.g., Lunati et al., 2002), and renormalization (e.g., Zhang, 1998). For example, the time evolution of a conservative solute dispersion has been investigated in detail for unimodal porous media (e.g., Dagan, 1989, Rajaram and Gelhar, 1993; Rubin et al., 1999; Fiori and Dagan, 2002). The time- and scale-

dependent effective retardation factor in a unimodal porous media was presented by Rajaram (1997) and in a hierarchical porous media by Deng et al. (2013) using a Lagrangian-based theory. The time evolution of reactive solute dispersion undergoing equilibrium sorption has been investigated by Bellin et al. (1993) and Bellin and Rinaldo (1995) for unimodal porous media. Samper and Yang (2006) analyzed the multicomponent cation exchange reactions in heterogeneous porous media (see also Yang and Samper, 2009). In this paper we use the Deng et al. (2013) conceptual model for porous media with hierarchical organization of reactive minerals (see Fig.1) and develop a Lagrangian-based theory to analyze the reactive solute dispersion undergoing equilibrium sorption.

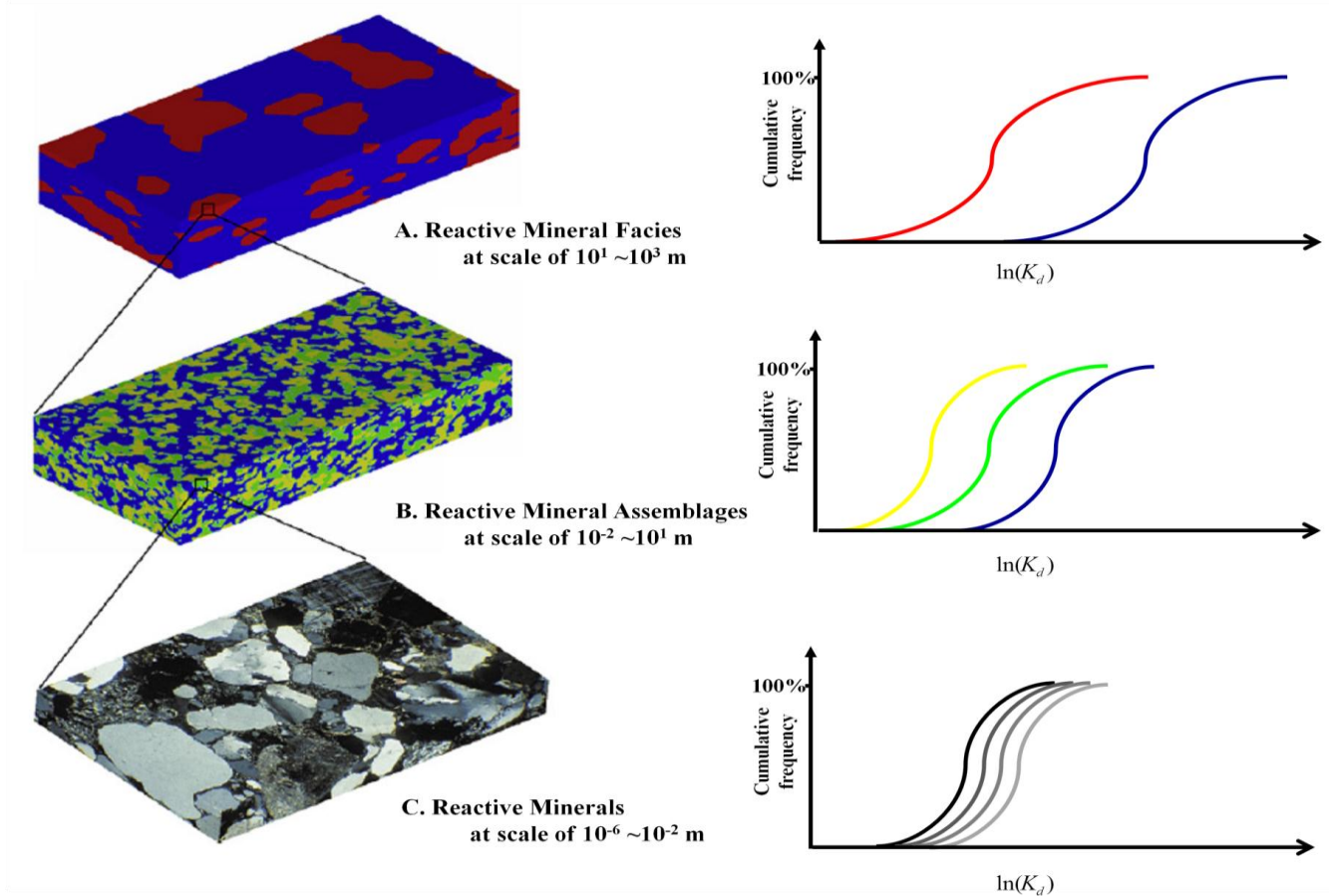


Fig. 1. Conceptual model for reactive mineral facies at different spatial scales, and corresponding modes for the log sorption distribution coefficient, $\ln(K_d)$. Modified from Deng et al. (2013).

Aquifer architecture is often conceptualized as a hierarchy with facies types defined at each scale comprising assemblages of facies types defined at a smaller scale, across any number of hierarchical levels (e.g. Bridge, 2006). Using the information about facies types defined at different scales can considerably simplify the task of characterizing subsurface heterogeneity. It has been shown that facies types at different scale control the scale-dependence of K and K_d (Allen King et al., 2006; Ritzi and Allen-King, 2007; Dai et al., 2004, 2005; Zhou et al., 2013; Gershenson et al., 2014). Importantly, K_d is known to vary with sedimentary facies types (Allen-King et al., 1998, 2006; Ritzi et al., 2013; Soltanian and Ritzi, 2014) and reactive mineral facies (Cheng et al., 2007; Deng et al., 2013). Information from sedimentary facies types and/or reactive mineral facies at different scales could be used in developing models for understanding reactive transport processes.

Facies classifications are not unique (Dai et al., 2005; Soltanian and Ritzi, 2014). What is important is that the classification should be useful, and usefulness depends upon context. Reactive minerals can be used to define facies for characterizing heterogeneity both in K and in K_d . The Deng et al. (2013) conceptual model is useful for geologic architecture within bedrock in which the type of reactive minerals and their spatial distributions exert the strongest control on the attributes of interest. Using this classification might not be appropriate for deposits where K does not co-vary with mineralogic facies controlling reactivity. We accept that the Deng et al. (2013) classification is useful for geologic architecture within certain settings and our goal is to derive a Lagrangian-based theory using their classification for hierarchical organization of reactive minerals. To our knowledge, there is no theory available for analyzing reactive solute dispersion in hierarchical porous media with hierarchical organization of reactive minerals. Note

that the theory developed in this paper can be extended to any type of system classification. In developing the theory we follow Rajaram (1997) which is different in part from the Lagrangian-based model presented by Bellin et al. (1993). Here the theory is developed in a formation with multiple K and K_d modes and hierarchical organization across scales. Note that while Bellin et al. (1993) represented three-dimensional isotropic formations with one scale of spatial variability, in this study we derived a model for three-dimensional anisotropic formations.

In section 2 we briefly review the Deng et al. (2013) conceptual model for hierarchical multimodal porous media with reactive minerals. Section 3 presents the derivation of a Lagrangian-based theory for reactive solute dispersion. In section 4 an example is used to illustrate the utility of the developed theory.

Conceptual model for hierarchical multimodal porous media and geostatistical characterization

Aside from aqueous-phase chemical species and physiochemical conditions such as temperature and pH, the sorption reactions in porous media depends on types of reactive minerals and their spatial distributions (Deng et al., 2010, 2013). Mineral reactivity is defined in terms of sorption/desorption process. Deng et al. (2013) presented a conceptual model of reactive minerals in quartz-feldspar sandstone with multimodal $\ln(K_d)$ and $\ln(K)$ subpopulations. In their conceptual model mineral facies have a hierarchical organization and there is a corresponding hierarchy of $\ln(K_d)$ subpopulations (see Fig.1). In the hierarchy, the reactive minerals (RMs) constitute reactive mineral assemblages (RMAs), which, in turn, form reactive mineral facies (RMFs). Here we briefly review the hierarchy of reactive minerals.

The base of the hierarchical organization of reactive minerals is the microform scale (10^{-6} to 10^{-2} m). The microform scale is associated with RMs. This scale is related to the scale of mineral grains in a rock. RMs are minerals that are sensitive to a specified geochemical reaction. There is $\ln(K_d)$ subpopulations in each RM. Examples of RMs are calcite, smectite, and hematite which have different sorption coefficients (see also Zavarin et al., 2004). There are also non-reactive minerals (NRMs) with a large volume proportions in quartz-feldspar sandstone. These NRMs (e.g., quartz and feldspar) have low sorption capabilities. The second hierarchical level is the mesoform scale (10^{-2} to 10^1 m). The mesoform scale has RMAs with occurrences of both NRMs and RMs. Examples of RMAs are Clay-Quartz-feldspar, Clay-Fe₂O₃-Quartz-Feldspar, and Clay-Organic Mater-Quartz-Feldspar. The RMA composed of RMs has a multimodal structure for uranium sorption coefficients. Also, there can be one or several non-reactive mineral assemblages (NRMAs). The third hierarchical level is the macroform scale (10^1 to 10^3 m) with reactive mineral facies (RMF). These are a body of rock characterized by an association of RMAs (or RMAs and NRMA). Two types of RMFs are Calcite-Clay-Organic Matter (CCO-RMF) and Clay-Hematite could be found in sandstone. Similar to Deng et al. (2013), for the purpose of demonstration, only the CCO-RMF with three RMAs is used in this study, and thus flow and transport are assumed to occur within a CCO-RMF. The analysis can be easily extended to also include the RM scale. However, it is not in the scope of this study.

Consider a domain Ω filled with N number of RMA of mutually exclusive occurrences. Let $Y(x)$ be multimodal spatial random variables for $\ln(K)$ or $\ln(K_d)$ at location x . It can be expressed using indicator geostatistics as:

$$Y(x) = \sum_{j=1}^N I_j(x) Y_j(x) \quad (1)$$

where $I_j(x)$ is indicator variable within the domain Ω and $Y_j(x)$ are variables of the j -th RMA.

Following Ritzi et al. (2004), the composite mean M_Y and variance σ_Y^2 of $Y_j(x)$ are computed as

(see also Huang and Dai, 2008):

$$M_Y = \sum_{j=1}^N p_j m_j \quad (2)$$

$$\sigma_Y^2 = \sum_{j=1}^N p_j \sigma_j^2 + \frac{1}{2} \sum_{i=1}^N \sum_{j=1}^N p_j p_i (m_i - m_j)^2 \quad (3)$$

where p_j , m_j , and σ_j^2 are volumetric proportion, mean, and variance, respectively. The multimodal covariance function of $\ln(K)$ and $\ln(K_d)$ has been presented from previous studies

(see also Dai et al., 2004; and Soltanian et al., 2014):

$$C_Y(\xi) = \sum_{j=1}^N p_j^2 \sigma_j^2 e^{-\frac{\xi}{\lambda_j}} + \sum_{i=1}^N p_j (1 - p_j) \sigma_j^2 e^{-\frac{\xi}{\lambda_\phi}} + \frac{1}{2} \sum_{i=1}^N \sum_{j=1}^N p_i p_j (m_i - m_j)^2 e^{-\frac{\xi}{\lambda_i}} \quad (4)$$

where λ_j and λ_i are the integral scale of the j -th RMA unit and the indicator integral scale of the RMAs, respectively; $\lambda_\phi = \lambda_j \lambda_i / (\lambda_j + \lambda_i)$.

The Lagrangian-based theory

Spatial variability of velocity experienced by reactive solutes is the first step in characterizing reactive solute spreading (Bellin et al., 1993; Rajaram, 1997). The Lagrangian velocity for reactive solutes is as follows:

$$u(x) = \frac{v(x)}{R(x)} \quad (5)$$

where u is the reactive solute velocity, v is the groundwater velocity, and R is the retardation factor with a constant mean \bar{R} , variance σ_R^2 and a stationary spatial covariance $C_{RR}(\xi)$ (Bellin et al., 1993; Rajaram, 1997). For transport of a reactive solute with the linear equilibrium sorption assumption, spatial variability of R is related to the spatial variability of K_d by the relationship $R(x) = 1 + (\rho_b / n)K_d(x)$ where ρ_b and n are the bulk density and porosity of the medium, respectively. The perturbation of the reactive solute velocity, u'_i , is found by linearizing equation (5) as:

$$u'_i = \frac{v'_i}{R} - \frac{\bar{v}_i R'}{R^2} \quad (6)$$

where R' is the R perturbation, and v'_i is the perturbation of the groundwater velocity (Rajaram, 1997). Using equation (6), and the spectra of the flow velocity and the retardation factor ($S_{v_i v_i}$ and S_{RR}) and their cross-spectral density, $S_{v_i R}$, the spectral density of the reactive solute velocity is given by:

$$S_{u_i u_j}(k) = \frac{1}{R^2} S_{v_i v_j}(k) + \frac{\bar{v}_i \bar{v}_j}{R^4} S_{RR}(k) - \frac{\bar{v}_i}{R^3} S_{v_j R}(k) - \frac{\bar{v}_j}{R^3} S_{v_i R}(k) \quad (7)$$

where $k = (k_1, k_2, k_3)^T$ is a 3-D wave-number vector (Rajaram, 1997). Thus, the following relationship defines the covariance of reactive solute velocity:

$$C_{u_i u_j}(\xi) = \frac{1}{R^2} C_{v_i v_j}(\xi) + \frac{\bar{v}_i \bar{v}_j}{R^4} C_{RR}(\xi) - \frac{\bar{v}_i}{R^3} C_{v_j R}(\xi) - \frac{\bar{v}_j}{R^3} C_{v_i R}(\xi) \quad (8)$$

Following Dagan (1984, 1989) and Bellin et al. (1993) and using the Lagrangian-based theory the time-dependent dispersion tensor for a reactive solute, $\tilde{D}_{ij}^R(t)$, is found as:

$$\tilde{D}_{ij}^R(t) = \int_0^t C_{u_i u_j}(s) ds \quad (9)$$

We assume that the velocity covariance depends on the mean particle trajectory instead of the actual one. Therefore, ξ can be approximated by $\bar{v}_1 t / \bar{R}$. This assumption has been successfully used for analyzing the dispersion of nonreactive and reactive solutes (Dagan, 1989; Bellin et al., 1993; Bellin and Rinaldo, 1995; Dai et al., 2004).

Bellin et al. (1993) showed that the transverse retarded velocity is independent of the variability of R . Our focus is on analyzing the longitudinal dispersion of a reactive plume as has been observed in field experiments (Roberts et al., 1986; Garabedian et al., 1988). Therefore, we assume that the velocity field is uniform in average, and that the mean velocity is aligned with the x_1 axis such that $v = (v_1, 0, 0)$. Thus,

$$\begin{aligned} \tilde{D}_{11}^R(t) &= \int_0^t C_{u_1 u_1} \left(\frac{\bar{v}_1}{R} s \right) ds \\ &= \frac{1}{R^2} \int_0^t C_{v_1 v_1} \left(\frac{\bar{v}_1}{R} s \right) ds \quad (10a) \end{aligned}$$

$$+ \frac{\bar{v}_1^2}{R^4} \int_0^t C_{RR} \left(\frac{\bar{v}_1}{R} s \right) ds \quad (10b)$$

$$- \frac{2\bar{v}_1}{R^3} \int_0^t C_{v_1 R} \left(\frac{v_1}{R} s \right) ds \quad (10c)$$

Bellin et al. (1993) used both the cross-covariance of $\ln(K)$ and R , and the cross-covariance of the hydraulic head and R by performing first-order approximation in order to derive $C_{v_1 R}(\xi)$. Here we follow Rajaram (1997) in which $C_{v_1 R}(\xi)$ is derived directly from its spectral density, $S_{v_1 R}(k)$, using the cross-correlation between $\ln(K)$ and $\ln(K_d)$.

The retardation factor can also be expressed as $R(x) = 1 + (\rho_b / n)e^{w(x)}$ where w is $\ln(K_d)$.

Using stochastic theory w can be replaced by $\bar{w} + w'$ where \bar{w} and w' are the mean and the perturbation of w . Soltanian et al. (in revision) derived the following expression for the perturbation of R :

$$R' = R - \bar{R} = \frac{\rho_b}{n} K_d^G (e^{w'} - e^{\left[\frac{\sigma_w^2}{2}\right]}) \quad (11)$$

where K_d^G is the geometric mean of $K_d(x)$, and σ_w^2 is the variance of w . Using the Taylor series expansion for $e^{w'}$, we calculate C_{RR} approximately as:

$$C_{RR}(\xi) = \left(\frac{\rho_b}{n} K_d^G\right)^2 e^{\left[\frac{\sigma_w^2}{2}\right]} (e^{C_w(\xi)} - 1) \quad (12)$$

Therefore, the corresponding variance of the retardation factor is:

$$\sigma_R^2 = \left(\frac{\rho_b}{n} K_d^G\right)^2 e^{\left[\frac{\sigma_w^2}{2}\right]} (e^{\left[\frac{\sigma_w^2}{2}\right]} - 1) \quad (13)$$

Following Gelhar (1993), Rajaram (1997), and Deng (2013) the perturbation of v is obtained as:

$$v' = \frac{K^G J}{n} \left(1 - \frac{k_1^2}{k^2}\right) f \quad (14)$$

where f is the perturbation of $\ln(K)$.

Note that we used a nonlinear expansion for $\ln(K_d)$, equation (11), and first-order for $\ln(K)$, equation (14). Bellin et al. (1993) and Bellin and Rinaldo (1995) have used the same inconsistent expansion in order to analyze the time-dependent dispersion of reactive solutes (see equation (10a) and (17) in Bellin et al., 1993). Their results were tested against numerical

simulations and validated by Bosma et al. (1993) for relatively small variances (<1.6). Here we assume similarly small variances. Thus, the developed theory is valid for aquifers with mild heterogeneity contrast ($\sigma_f^2, \sigma_w^2 < 1$).

The $S_{v_1R}(k)$ is derived by using equations (11) and (14). The $S_{v_1R}(k)$ is found as:

$$S_{v_1R}(k) = \frac{\rho_b}{n^2} K^G K_d^G J \left(1 - \frac{k_1^2}{k^2}\right) f(e^{w'} - e^{\left[\frac{\sigma_w^2}{2}\right]}) \quad (15)$$

Using the Taylor series expansion for $e^{w'}$ and considering the point that the odd moments of a log normal distribution are zero, $S_{v_1R}(k)$ is found as:

$$S_{v_1R}(k) = \frac{\rho_b}{n^2} K^G K_d^G J \left(1 - \frac{k_1^2}{k^2}\right) \frac{\sinh(\sigma_w)}{\sigma_w} S_{fw}(k) \quad (16)$$

where $S_{fw}(k)$ is the spectral density of the fluctuations of $f - w$, and \sinh is hyperbolic sine function.

The K and K_d are assumed to be perfectly correlated as $\ln(K_d) = a \ln(K) + b$, where a and b are real constants. Then the cross-spectral density of $\ln(K)$ and $\ln(K_d)$ has a linear relationship given by $\ln(K)$, i.e. $S_{fw}(k) = a S_{ff}(k)$. Therefore, $S_{v_1R}(k)$ is expressed as:

$$S_{v_1R}(k) = \frac{\rho_b}{n^2} K^G K_d^G J a \frac{\sinh(\sigma_w)}{\sigma_w} \left(1 - \frac{k_1^2}{k^2}\right) S_{ff}(k) \quad (17)$$

Using equation (14) $S_{v_1v_1}(k)$ is easily found as follows:

$$S_{v_1v_1}(k) = \left(\frac{K^G J}{n}\right)^2 \left(1 - \frac{k_1^2}{k^2}\right)^2 S_{ff}(k) \quad (18)$$

The relationship between the spectral density and the covariance function is expressed as follows:

$$S(k) = \frac{1}{(2\pi)^3} \iiint_{-\infty}^{\infty} e^{-ik \cdot \xi} C(\xi) d\xi \quad (19)$$

The $C_{v_1 v_1}(\xi)$ and $C_{v_1 R}(\xi)$ are used in form of their spectral density to find the longitudinal dispersion of a reactive solute. Therefore, equation (10) can be rewritten as follows:

$$\begin{aligned} \tilde{D}_{11}^R(t) &= \int_0^t C_{u_1 u_1} \left(\frac{v_1}{R} s \right) ds \\ &= \frac{1}{R^2} \int_0^t \iiint_{\Omega} e^{-ik \frac{\bar{v}_1}{R} s} S_{v_1 v_1}(k) ds dk \quad (20a) \end{aligned}$$

$$+ \frac{\bar{v}_1^2}{R^4} \int_0^t C_{RR} \left(\frac{\bar{v}_1}{R} s \right) ds \quad (20b)$$

$$- \frac{2\bar{v}_1}{R^3} \int_0^t \iiint_{\Omega} e^{-ik \frac{\bar{v}_1}{R} s} S_{v_1 R}(k) ds dk \quad (20c)$$

By substituting equations (12), (17), and (18) into equation (20) and using equation (4) to represent the multimodal covariance function of $\ln(K)$ and $\ln(K_d)$, the final expression for longitudinal dispersivity of a reactive solute in multimodal porous media is found as:

$$\begin{aligned} \alpha_{11}^R(t) &= \frac{\tilde{D}_{11}^R(t) \bar{R}}{\bar{v}_1} = \sum_{j=1}^N p_j^2 \sigma_{f_i}^2 \lambda_i F_1(\lambda_i) + \sum_{j=1}^N p_j (1-p_j) \sigma_{f_i}^2 \lambda_{\varphi} F_1(\lambda_{\varphi}) + \frac{1}{2} \sum_{i=1}^N \sum_{j=1}^N p_i p_j (m_{f_i} - m_{f_j})^2 \lambda_i F_1(\lambda_i) \\ &+ \frac{\bar{v}_1}{R^3} \left(\frac{\rho_b}{n} K_d^G \right)^2 e^{[\sigma_w^2]} \left(\int_0^t \left(e^{\sum_{j=1}^N p_j^2 \sigma_{w_j}^2 e^{-\frac{\bar{v}_1}{R \lambda_i} s}} + \sum_{j=1}^N p_j (1-p_j) \sigma_{w_j}^2 e^{-\frac{\bar{v}_1}{R \lambda_{\varphi}} s} + \frac{1}{2} \sum_{i=1}^N \sum_{j=1}^N p_i p_j (m_{w_i} - m_{w_j})^2 e^{-\frac{\bar{v}_1}{R \lambda_i} s} - 1 \right) ds \right) \\ &- \frac{2}{R} \frac{\rho_b}{n^2} K^G K_d^G J a \frac{\sinh(\sigma_w)}{\sigma_w} \left\{ \sum_{j=1}^N p_j^2 \sigma_{f_i}^2 \lambda_i F_2(\lambda_i) + \sum_{j=1}^N p_j (1-p_j) \sigma_{f_i}^2 \lambda_{\varphi} F_2(\lambda_{\varphi}) \right. \\ &\left. + \frac{1}{2} \sum_{i=1}^N \sum_{j=1}^N p_i p_j (m_{f_i} - m_{f_j})^2 \lambda_i F_2(\lambda_i) \right\} \quad (21) \end{aligned}$$

where

$$F_1(\lambda) = \{1 - e^{-\tau} - \varepsilon \int_0^{\infty} 2r J_1(\beta) \frac{2u^{\frac{3}{2}} - \varepsilon r(v + 2u)}{v^2 u^{\frac{3}{2}}} + \left[\frac{(2 - \beta^2)J_1(\beta) - \beta J_0(\beta)}{r\tau^2} \right] \left[\frac{\varepsilon^3 r^3 (v + 4u) + u^{\frac{3}{2}}(5v - 4u)}{v^3 u^{\frac{3}{2}}} \right] dr \},$$

$$F_2(\lambda) = \{1 - e^{-\tau} - 2\varepsilon^2 \int_0^{\infty} r^2 \left[\frac{1}{2vu^{\frac{3}{2}}} + \frac{1}{v^2 u^{\frac{1}{2}}} - \frac{1}{v^2 \varepsilon r} \right] J_1(\beta) dr \},$$

$$\beta = r\tau,$$

$$u = 1 + r^2,$$

$$v = 1 + r^2 - \varepsilon^2 r^2,$$

$$\tau = \frac{\bar{v}_1 t}{R\lambda},$$

Also, ε is the anisotropy ratio is defined as the vertical integral scale of the hydraulic conductivity to the horizontal component. The J_0 and J_1 are the zero and first order Bessel functions, respectively. The integration method to find equation (21) can be found in Appendix A, B, C, and D. The expressions in equation (21) cannot be integrated in closed form. We use the quadrature method in order to numerically integrate and evaluate equation (21) at a number of points in the parameter space, and present the results in Section 4.

Results and Discussion

In order to analyze the reactive solute dispersion using the developed Lagrangian-based model, we use an example presented by Deng et al. (2013) as summarized in Table 1. In this example the parameter values of the three RMAs are extracted from a real case.

Table 1. Parameters from the example used by Deng et al. (2013).

RMF	RMA	L_j	p_j	Parameters	m_j	σ_j^2	M_j^G	λ_j	λ_φ	R_j
Cc-Clay-OM	Cc-QF	50.0	0.6	$\ln K$	1.5	0.6	4.48	10	6.67	2.39
RMF				$\ln K_d$	-2.2	0.22	0.11	12	7.5	
	Clay-Fe ₂ O ₃ -QF	23.5	0.15	$\ln K$	0.5	0.3	1.65	6	4.62	4.76
				$\ln K_d$	-1.2	0.12	0.3	8	5.71	
	Clay-OM-QF	26.7	0.25	$\ln K$	0.05	0.15	1.05	9	6.21	10.26
				$\ln K_d$	-0.3	0.1	0.74	7	5.19	
	Parameters	$\ln K$			$\ln K_d$			R		
	Statistics	M_Y	σ_Y^2	M_Y^G	M_Y	σ_Y^2	M_Y^G	M_Y	σ_Y^2	M_Y^G
	Values	0.99	0.86	2.68	-1.58	0.84	0.21	4.93	20.25	3.59
	Parameters	\bar{v}_1	$\sigma_{v,R}^2$		λ_T	n	ρ_b	J		
	Values	0.21	0.228		20.0	0.2	2.5	0.01		

Note: RMA = reactive mineral assemblage within a reactive mineral facies (RMF), Cc = calcite, Fe₂O₃ = iron oxides, QF = quartz and feldspar; For j -th RMA ($j = 1, 2, 3$), L_j = facies mean length (m), M_j^G = geometric mean, λ_j = correlation length (m), $\lambda_\varphi = \lambda_i \lambda_j / (\lambda_i + \lambda_j)$, R_j = retardation factor; M_Y = global mean, σ_Y^2 = global variance, M_Y^G = global geometric mean, \bar{v}_1 = mean flow velocity (m/d), $\sigma_{v,R}^2$ = cross-covariance of flow velocity and retardation factor, λ_T = indicator correlation length (m), n = porosity, ρ_b = bulk density of the porous media (g/cm³), J = average hydraulic gradient, K = hydraulic conductivity (m/d), K_d = sorption coefficient (cm³/g).

The $\alpha_{11}^R(t)$ is plotted in Fig.2 for three cases of correlation between $\ln(K)$ and $\ln(K_d)$: positively correlated ($a = 1$), uncorrelated ($a = 0$), and negatively correlated ($a = -1$). The $\alpha_{11}^R(t)$ increases monotonically with time for all cases. Fig.2 shows that the values of $\alpha_{11}^R(t)$ for the negatively correlated case are larger than those of the uncorrelated and positively correlated cases. In all cases the value of $\alpha_{11}^R(t)$ converges to a constant value when time is sufficiently large. Fig.2 also shows the influence of anisotropy ratio, ε , on $\alpha_{11}^R(t)$. It is observed that ε has a relatively small impact upon dispersion of reactive solutes in this example. The $\alpha_{11}^R(t)$ is slightly enhanced at early times by a smaller ε due to lateral mass transfer between streamlines with different velocities located adjacent to each other (Rubin, 2003). Furthermore, as shown in section 4, heterogeneity in $\ln(K_d)$ has a relatively larger impact on reactive solute transport than $\ln(K)$ heterogeneity or its anisotropy ratio.

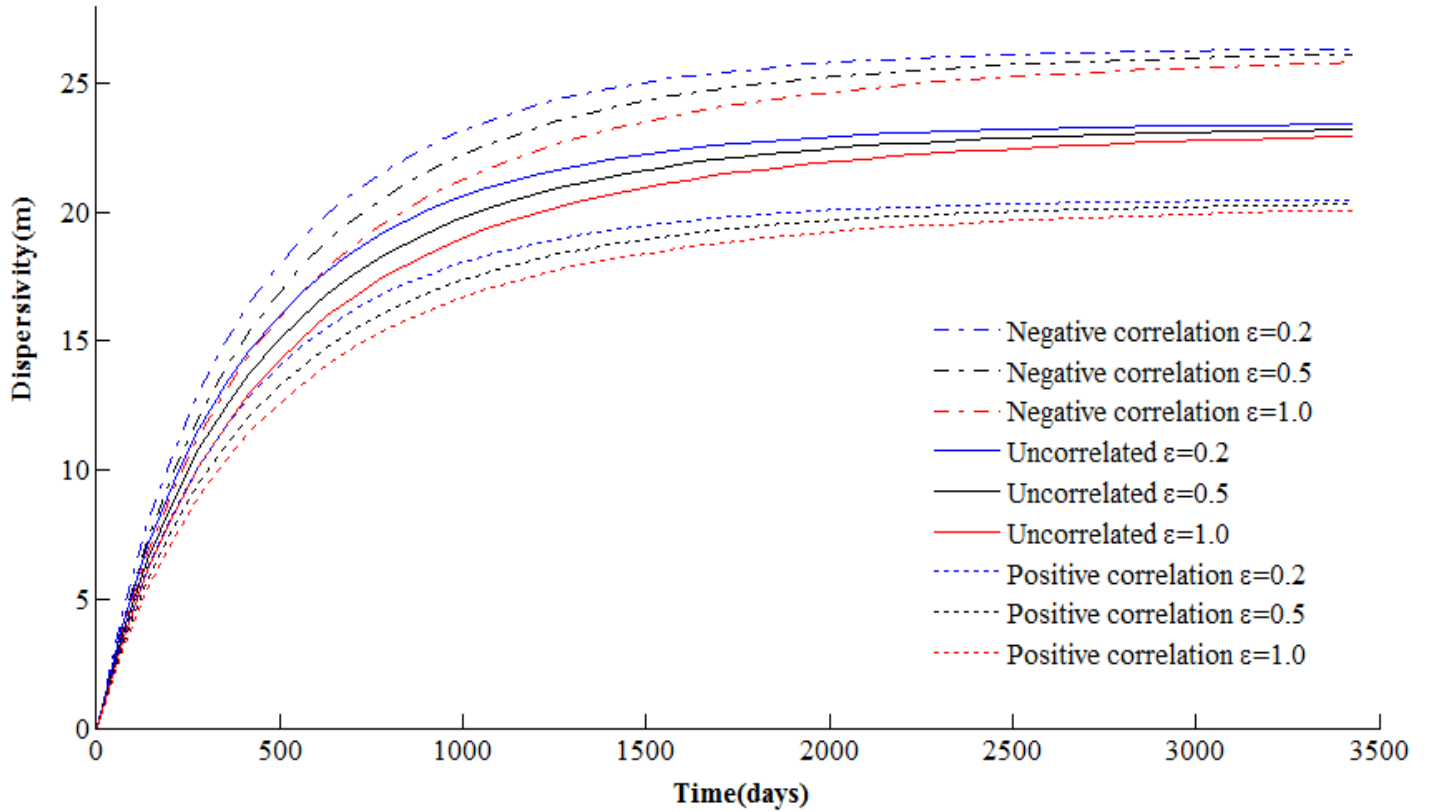


Fig. 2. The longitudinal dispersivity $\alpha_{11}^R(t)$ for a porous medium with three RMFs. Three different cases with positive correlation ($a=1$), no correlation ($a=0$), and negative correlation ($a=-1$) are shown. The influence of the anisotropy ratio, ϵ , for all of the three cases is presented.

Fig. 3 shows $\alpha_{11}^R(t)$ changes with the indicator correlation length (λ_l) when the time is fixed at 1000 d. In all cases $\alpha_{11}^R(t)$ increases to a maximum at about $\lambda_l=300$ m, and then it stays constant. Although $\alpha_{11}^R(t)$ reaches a maximum for three cases, it reaches different values. This reflects the contribution from the cross-correlation between R and v_1 , represented by equation (20c).

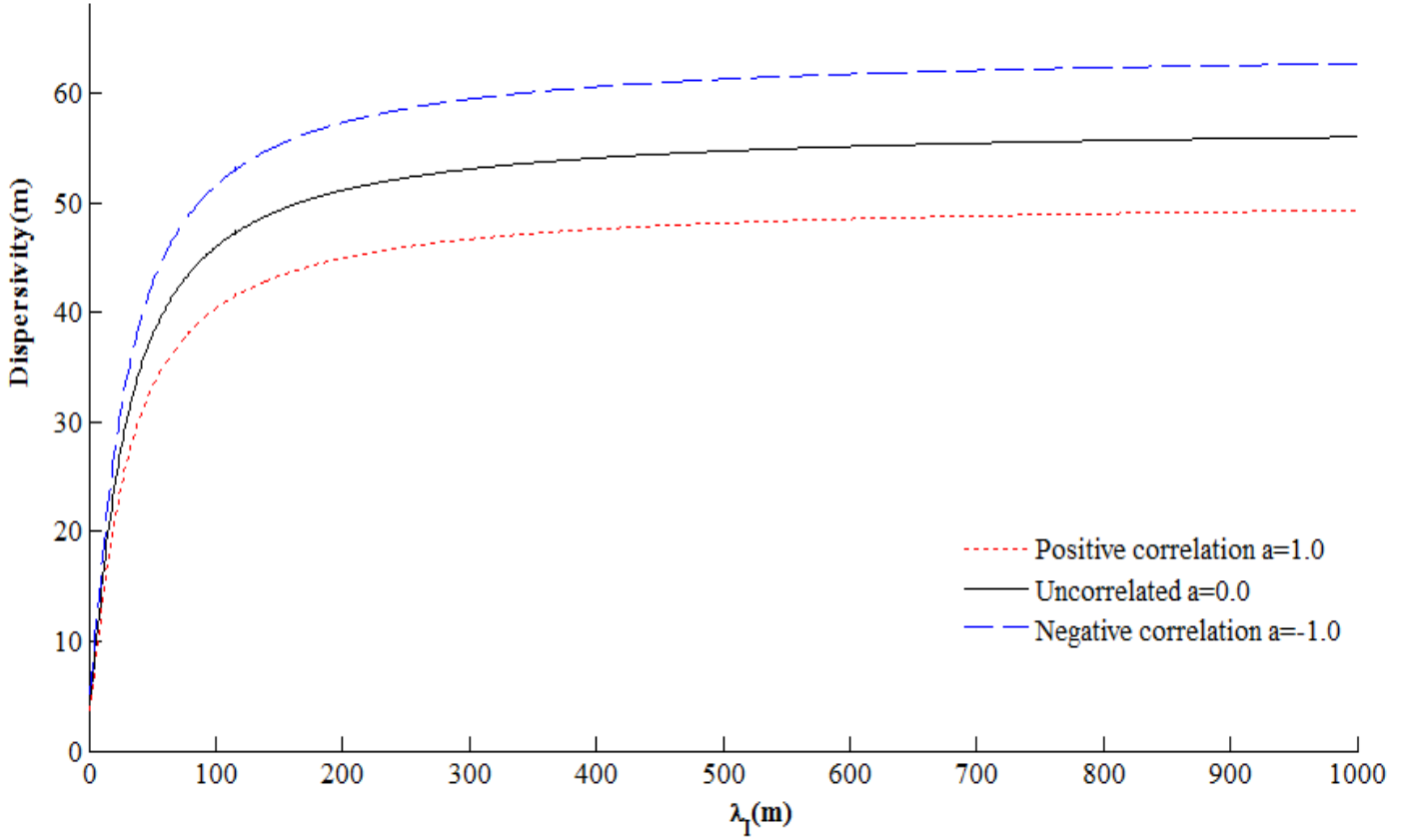


Fig. 3. The longitudinal dispersivity $\alpha_{11}^R(t)$ changes with indicator correlation length when time is fixed at 1000 d. Three different cases with positive correlation ($a=1$), no correlation ($a=0$), and negative correlation ($a=-1$) are shown. The anisotropy ratio, ε , is 1.

In order to better understand the impact of heterogeneity in both $\ln(K)$ and $\ln(K_d)$ on reactive solute dispersion we study the effect of changing the mean, variance, and integral scale of $\ln(K)$ and $\ln(K_d)$ for each RMA below.

The impact of $\ln(K)$ heterogeneity

The influence of changing the mean of log hydraulic conductivity (m_j) for each RMA is shown in Fig. 4A. We set m_j between -2.5 and 2.5 and time is fixed at 1000 d. Fig. 4A shows that any changes in values of mean of hydraulic conductivity can affect $\alpha_{11}^R(t)$. However, it

depends on the type of RMA. For example, decreasing the mean hydraulic conductivity for RMA1 does not significantly affect $\alpha_{11}^R(t)$ for both positive and negative correlation, whereas $\alpha_{11}^R(t)$ can increase if the mean of hydraulic conductivity for RMA 1 increases. For RMA 2, by decreasing the mean of hydraulic conductivity $\alpha_{11}^R(t)$ increases. The same is true for RMA 3. Note that RMA 1 has the largest variance and mean of hydraulic conductivity and the smallest mean sorption. In contrast, RMA 3 has the smallest variance and mean of hydraulic conductivity and the largest mean sorption coefficient.

Fig. 4B illustrates how changes in variances of log hydraulic conductivity for RMAs can affect $\alpha_{11}^R(t)$ when the time is fixed at 1000 d. Increases in variance of hydraulic conductivity for all RMAs lead to a linear increase in $\alpha_{11}^R(t)$. The dispersivity is more sensitive to changes in variance of log hydraulic conductivity for RMA1 than other two RMAs which can be attributed to the fact that RMA1 has the largest volume proportion. The $\alpha_{11}^R(t)$ is more sensitive to changes in variance of log hydraulic conductivity for RMA 3 than RMA 2 because the volume proportion of RMA 3 is slightly larger than RMA 2.

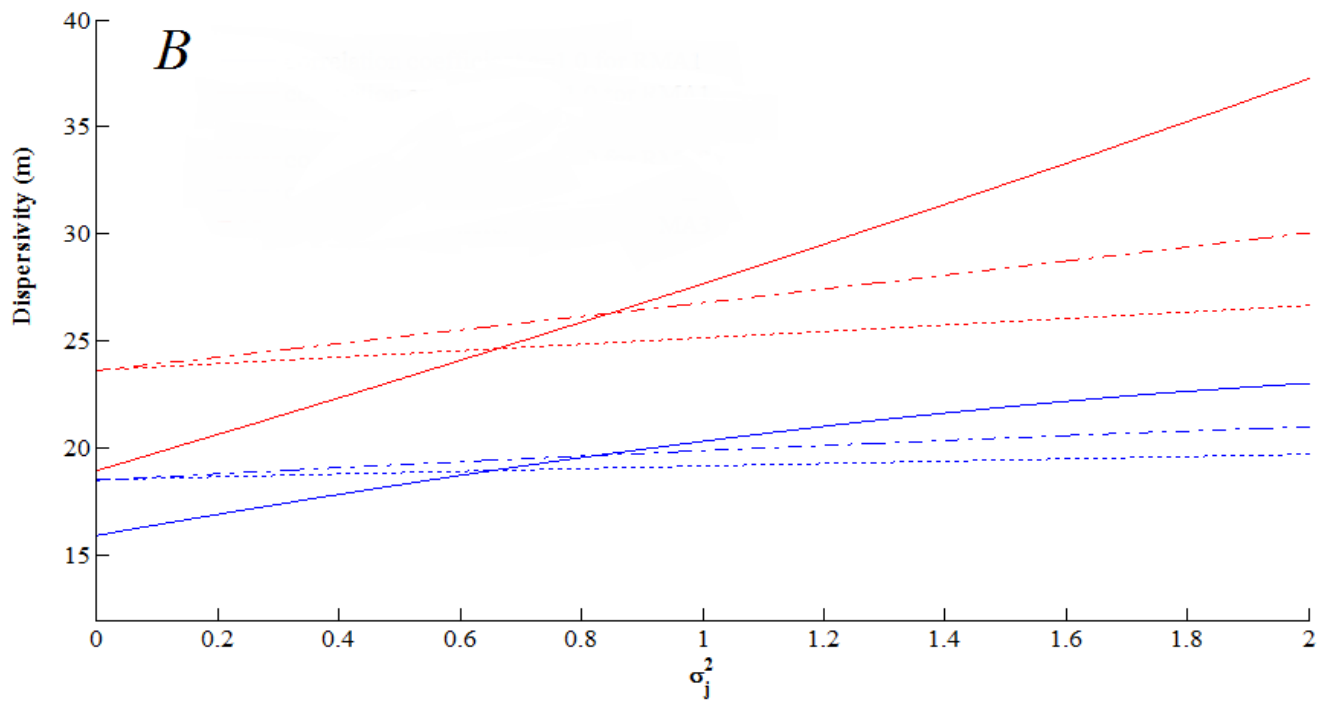
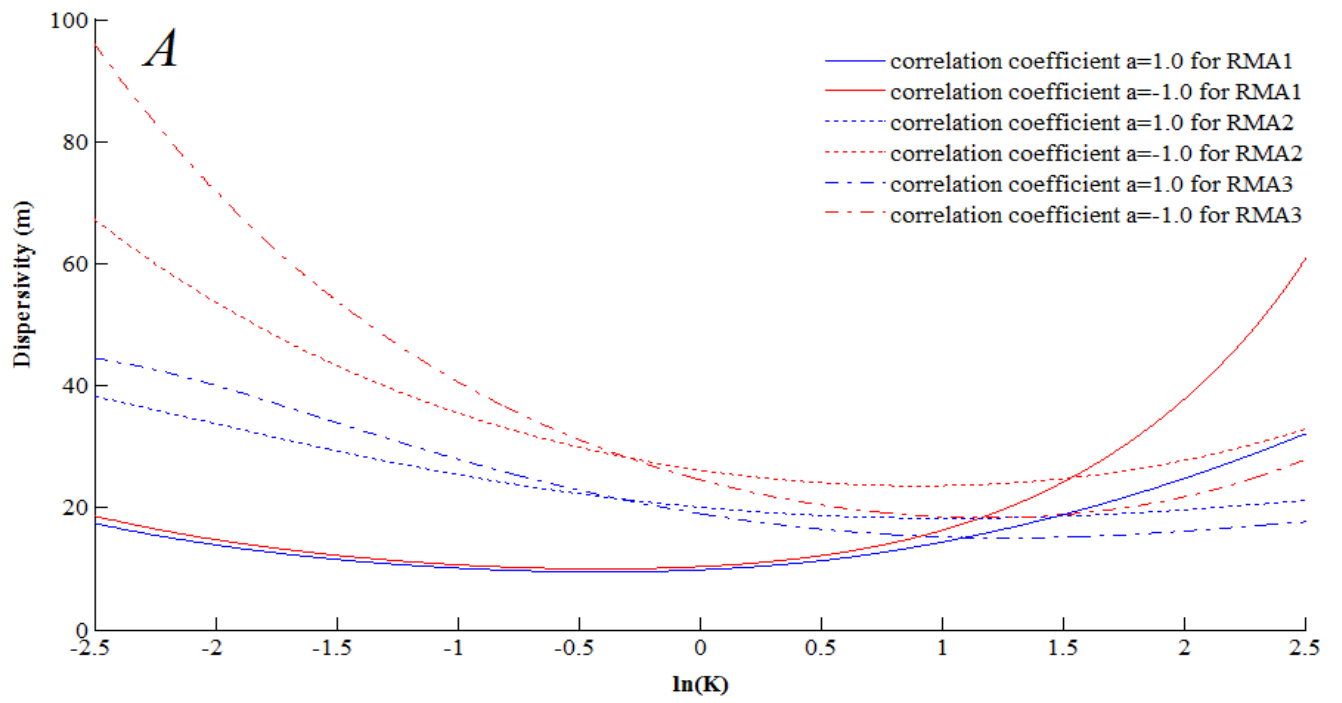
Fig. 4C shows $\alpha_{11}^R(t)$ changes with integral scales of log hydraulic conductivity when time is fixed at 1000 d. The changes in integral scales of log hydraulic conductivity for RMA 2 and 3 only produce a very small change in $\alpha_{11}^R(t)$. In contrast, for RMA1 it produces a large change in $\alpha_{11}^R(t)$ with a maximum at about $\lambda_j=300$ m, and then it remains constant. Therefore, $\alpha_{11}^R(t)$ is more sensitive to the integral scale of log hydraulic conductivity for RMA 1 because it has the largest volume proportion and also the largest integral scale.

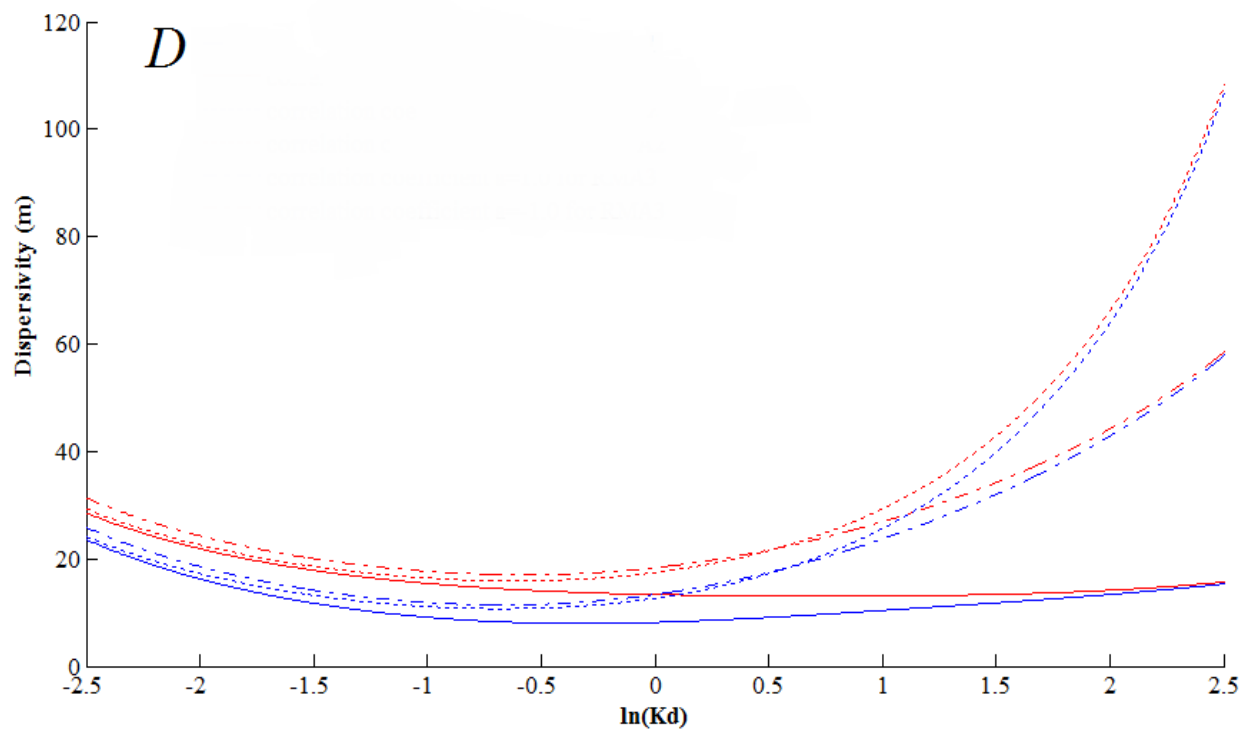
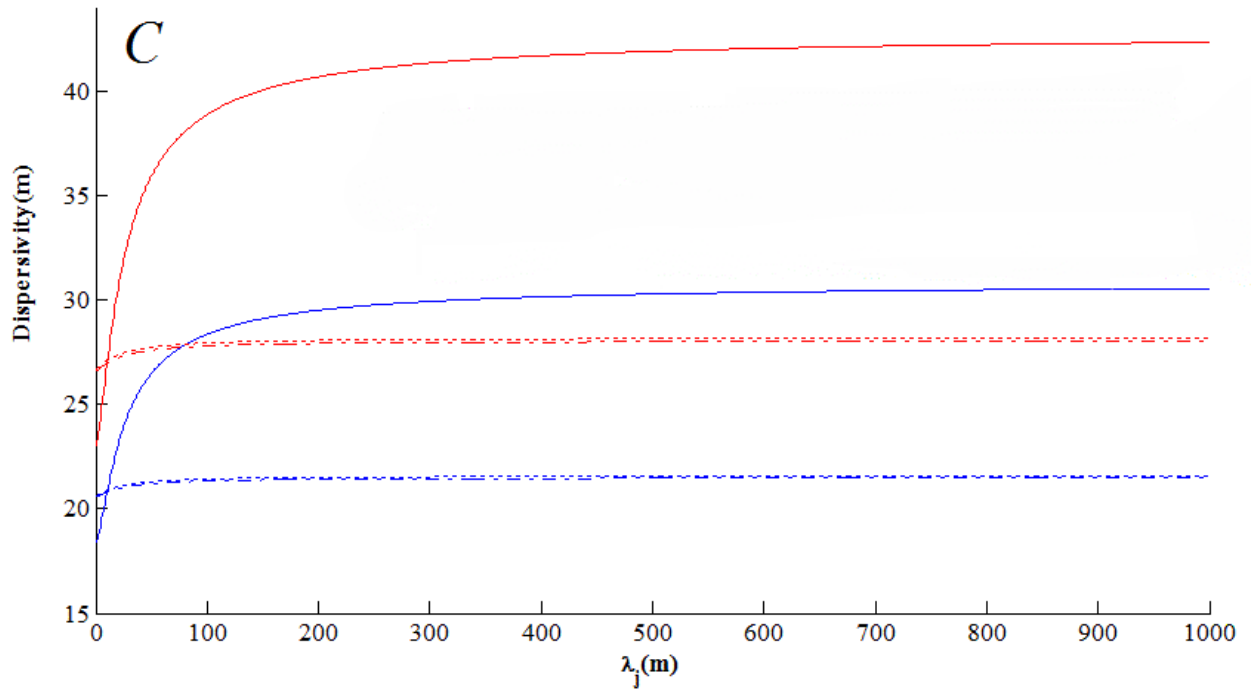
The impact of $\ln(K_d)$ heterogeneity

Fig. 4D shows how $\alpha_{11}^R(t)$ changes with the mean log sorption distribution coefficient when time is fixed at 1000 d. In general, increases from -2.5 to 0 result in slight decreases in $\alpha_{11}^R(t)$. However, increases from 0 to 2.5 lead to increases $\alpha_{11}^R(t)$, more for RMA 2 and 3.

Fig. 4E illustrates how the changes in the variance of the log sorption distribution coefficient for RMAs affect $\alpha_{11}^R(t)$ when the time is fixed at 1000 d. Increases in variances of the sorption distribution coefficient for all RMAs lead to increases in $\alpha_{11}^R(t)$. In contrast to changing the variance of $\ln(K)$, increasing the variance of $\ln(K_d)$ leads to nonlinear increases in $\alpha_{11}^R(t)$. By comparing Fig. 4E to Fig. 4B it is clear that $\alpha_{11}^R(t)$ is more sensitive to changes in the variance of the log sorption distribution coefficient for RMAs than the variance of the log hydraulic conductivity for RMAs.

Fig. 4F shows $\alpha_{11}^R(t)$ changes with the integral scales of the log sorption distribution coefficient when time is fixed at 1000 d. The $\alpha_{11}^R(t)$ is sensitive to changes in the integral scale of the log sorption distribution coefficient for RMA 1 which has the largest volume proportion and also the largest integral scale.





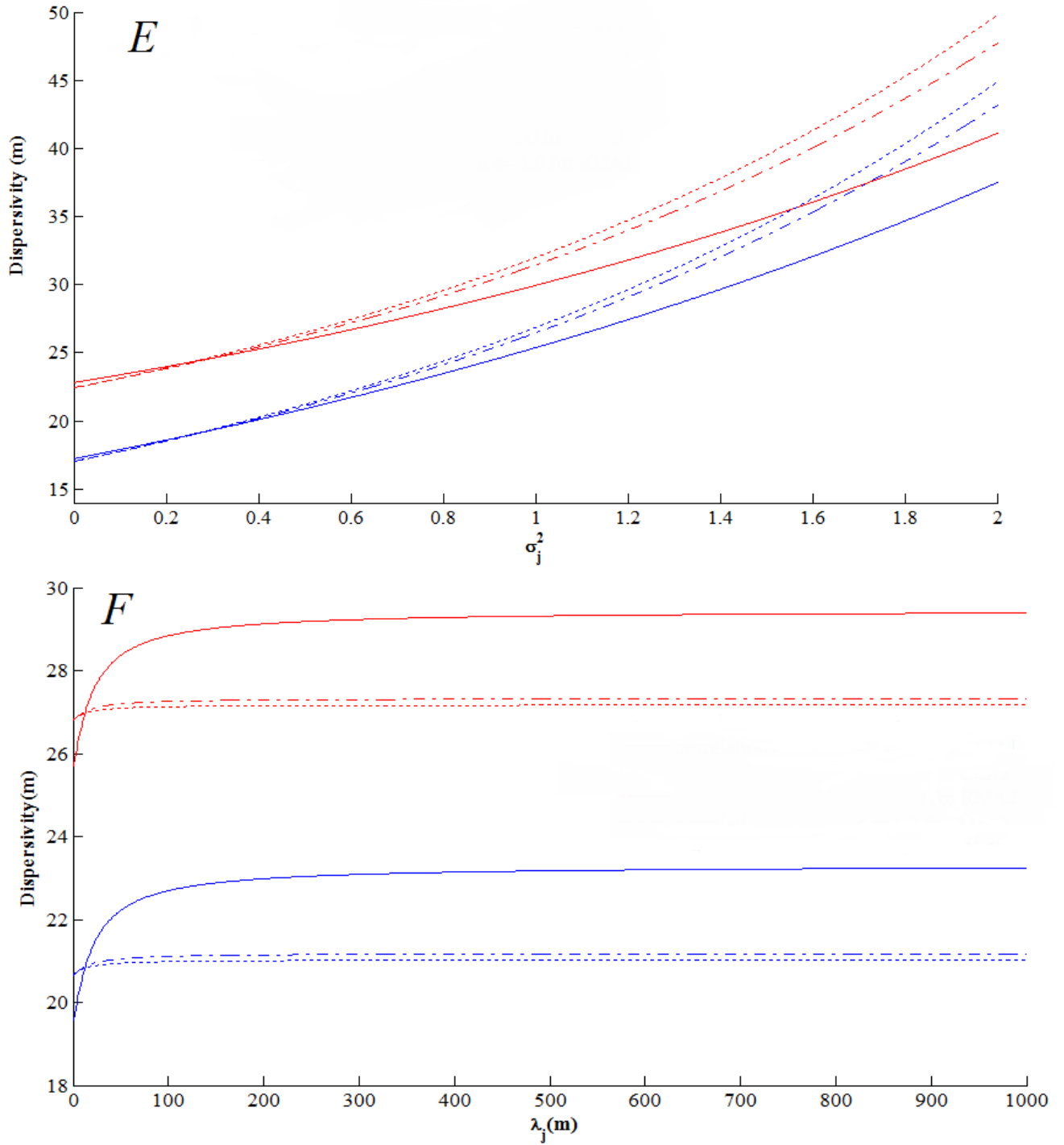


Fig. 4. The longitudinal dispersivity $\alpha_{11}^R(t)$ changes with (A) the mean hydraulic conductivity; (B) the variance of the hydraulic conductivity; (C) the integral scale of hydraulic conductivity; (D) the mean of the sorption distribution coefficient; (E) the variance of the sorption distribution coefficient; (F) the integral scale of the sorption distribution coefficient. Two different cases with

positive correlation ($a=1$) and negative correlation ($a=-1$) are shown for each RMA. Time at 1000 d. Anisotropy ratio, ε , is 1.

Conclusions

We developed a Lagrangian-based theory for analyzing the time-dependent reactive solute dispersion in hierarchical porous media with multimodal reactive mineral facies. This study demonstrates that the cross-correlation between K and K_d has a large impact on the longitudinal dispersivity $\alpha_{11}^R(t)$. The scale-dependence of reactive solute dispersion originated from heterogeneity in both K and K_d and their cross-correlation.

We considered three types of cross-correlation: perfectly positive cross-correlation, perfectly negative cross-correlation, and no cross-correlation. The positive cross-correlation reduces the reactive solute dispersivity, since heterogeneities in K and K_d counteract each other, which means that low K regions occurs with low retardation or high K regions occurs with high retardation. The negative cross-correlation causes an opposite effect. The results also indicate that anisotropy ratio does not significantly affect the transport of reactive solutes undergoing equilibrium sorption in the example used.

Furthermore, reactive solute dispersion is scale-dependent but not a linear function of the indicator correlation scale. We also performed analyses of sensitivity to changes in the integral scales of $\ln(K)$ and $\ln(K_d)$, and in the means and variances of $\ln(K)$ and $\ln(K_d)$ for each reactive mineral assemblage. The results show that heterogeneity in both $\ln(K)$ and $\ln(K_d)$ can significantly affect $\alpha_{11}^R(t)$. The $\alpha_{11}^R(t)$ is very sensitive to changes in mean and variance of both

$\ln(K)$ and $\ln(K_d)$. The $\alpha_{11}^R(t)$ is most sensitive to changes of integral scales of $\ln(K)$ and $\ln(K_d)$ for the reactive mineral assemblage with a larger volume proportion.

Appendix A. Derivation of spectral density of fluctuations in $\ln(K)$

Considering an exponential covariance function of $\ln(K)$:

$$C_{ff}(\xi) = \sigma_f^2 e^{-\left|\frac{\xi}{\mu}\right|} = \sigma_f^2 e^{-\sqrt{\left(\frac{\xi_1}{\mu_1}\right)^2 + \left(\frac{\xi_2}{\mu_2}\right)^2 + \left(\frac{\xi_3}{\mu_3}\right)^2}} \quad (\text{A1})$$

where μ_i are integral scale. The spectral density of $\ln(K)$ is evaluated by taking the Fourier transform of equation (19). Substituting (A1) into (19), then it yields:

$$S(k) = \frac{1}{(2\pi)^3} \int \int \int_{-\infty}^{\infty} e^{-ik \cdot \xi} \sigma_f^2 e^{-\left|\frac{\xi}{\mu}\right|} d\xi \quad (\text{A2})$$

Integrating (A2) leads to the following expression for spectral density of $\ln(K)$:

$$S_{ff}(k) = \frac{\sigma_f^2 \mu_1 \mu_2 \mu_3}{\pi^2} \frac{1}{(1 + (\mu k)^2)^2} \quad (\text{A3})$$

where $(\mu k)^2 = (\mu_1 k_1)^2 + (\mu_2 k_2)^2 + (\mu_3 k_3)^2$. Note that (A3) is also used for spectral density of $\ln(K_d)$.

Appendix B. Derivation of equation (20a)

Equation (20 a) contains the following integral:

$$(20a) = \frac{1}{R^2} \int_0^t C_{v_1 v_1} \left(\frac{\bar{v}_1}{R} s, 0, 0 \right) ds$$

Based on equation (18) we can write the following:

$$S_{v_1 v_1}(k) = \left(\frac{K^G J}{n}\right)^2 \left(1 - \frac{k_1^2}{k^2}\right)^2 S_{ff}(k) = \bar{v}_1^2 \left(1 - \frac{k_1^2}{k^2}\right)^2 S_{ff}(k) = \frac{v_1^2 \sigma_f^2 \mu_1 \mu_2 \mu_3}{\pi^2} \left(1 - \frac{k_1^2}{k^2}\right)^2 \frac{1}{(1 + (\mu k)^2)^2}$$

Therefore,

$$C_{v_1 v_1}(\xi) = \frac{\bar{v}_1^2 \sigma_f^2 \mu_1 \mu_2 \mu_3}{\pi^2} \int_{-\infty}^{\infty} \int_{-\infty}^{\infty} \int_{-\infty}^{\infty} \left(1 - \left(\frac{k_1}{k}\right)^2\right)^2 \frac{1}{(1 + (\mu k)^2)^2} \cos(k \cdot \xi) dk$$

Hence,

$$\begin{aligned} C_{v_1 v_1}\left(\frac{\bar{v}_1}{R} s, 0, 0\right) &= \frac{\bar{v}_1^2 \sigma_f^2 \mu_1 \mu_2 \mu_3}{\pi^2} \int_{-\infty}^{\infty} \int_{-\infty}^{\infty} \int_{-\infty}^{\infty} \left(1 - \left(\frac{k_1}{k}\right)^2\right)^2 \frac{1}{(1 + (\mu k)^2)^2} \cos\left(k_1 \frac{\bar{v}_1}{R} s\right) dk \\ &= \frac{\bar{v}_1^2 \sigma_f^2}{\pi^2} \int_{-\infty}^{\infty} \int_{-\infty}^{\infty} \int_{-\infty}^{\infty} \left(\frac{\mu_2^{-2} k_2^2 + \mu_3^{-2} k_3^2}{\mu_1^{-2} k_1^2 + \mu_2^{-2} k_2^2 + \mu_3^{-2} k_3^2}\right)^2 \frac{1}{(1 + k^2)^2} \cos\left(k_1 \frac{\bar{v}_1}{R} s\right) dk \end{aligned}$$

Changing variables $s' = \mu_1^{-1} \bar{R}^{-1} \bar{v}_1 s$ and $\tau = \bar{v}_1 t / \mu_1 \bar{R}$ gives:

$$(20a) = \frac{\bar{v}_1}{R} \frac{\sigma_f^2 \mu_1}{\pi^2} \int_0^{\tau} \int_{-\infty}^{\infty} \int_{-\infty}^{\infty} \int_{-\infty}^{\infty} \left(\frac{\mu_2^{-2} k_2^2 + \mu_3^{-2} k_3^2}{\mu_1^{-2} k_1^2 + \mu_2^{-2} k_2^2 + \mu_3^{-2} k_3^2}\right)^2 \frac{1}{(1 + k^2)^2} \cos(k_1 s') dk ds'$$

Now we have $\mu_1 = \mu_2 = \lambda$ and $\mu_3 = \varepsilon \lambda$ which ε is the anisotropy ratio. Thus,

$$(20a) = \frac{\bar{v}_1}{R} \frac{\sigma_f^2 \lambda}{\pi^2} \int_0^{\tau} \int_{-\infty}^{\infty} \int_{-\infty}^{\infty} \int_{-\infty}^{\infty} \left(1 - \frac{k_1^2}{k_1^2 + k_2^2 + \varepsilon^{-2} k_3^2}\right)^2 \frac{1}{(1 + k^2)^2} \cos(k_1 s) dk ds$$

Now changing to spherical coordinate system and defining:

$$\begin{aligned} k_1 &= r \cos \beta, \quad k_2 = r \sin \beta, \quad k_3 = k_3 \\ dk_1 dk_2 dk_3 &= r dr d\theta dk_3 \end{aligned}$$

Therefore,

$$(20a) = \frac{\bar{v}_1}{R} \frac{\sigma_f^2 \lambda}{\pi^2} \int_0^\tau ds \int_0^\infty r dr \int_0^{2\pi} d\theta \int_{-\infty}^\infty \left(1 - \frac{r^2 \cos^2 \theta}{r^2 + \varepsilon^{-2} k_3^2}\right)^2 \frac{\cos(sr \cos \theta)}{(1 + r^2 + k_3^2)^2} dk_3 \quad (\text{B1})$$

In order to derive the above integral the following general integrals are used:

$$\int_{-\infty}^\infty \frac{1}{(a^2 + x^2)^2} dx = \frac{\pi}{2a^3} \quad (\text{B2a})$$

$$\int_{-\infty}^\infty \frac{1}{(a^2 + x^2)^2 (b^2 + x^2)} dx = \frac{\pi}{2(b^2 - a^2)a^3} - \frac{\pi}{(b^2 - a^2)^2} \left(\frac{1}{a} - \frac{1}{b}\right) \quad (\text{B2b})$$

$$\int_{-\infty}^\infty \frac{1}{(a^2 + x^2)^2 (b^2 + x^2)^2} dx = \frac{\pi}{2(b^2 - a^2)^2} \left(\frac{1}{a^3} + \frac{1}{b^3}\right) - \frac{\pi}{(b^2 - a^2)^3} \left(\frac{1}{a} - \frac{1}{b}\right) \quad (\text{B2c})$$

In case of integral in (B1) the following parameters are used in (B2a)-(B2c):

$$a = 1 + r^2 = u,$$

$$b = \varepsilon r,$$

$$a^2 - b^2 = 1 + r^2 - \varepsilon^2 r^2,$$

Thus, one can derive (B1) as follows:

$$(20a) = \frac{\bar{v}_1 \sigma_f^2 \lambda}{R} \int_0^\tau ds \int_0^\infty \left\{ \frac{r}{2u^{\frac{3}{2}}} A(sr) dr + 2\varepsilon^2 r^3 \left[\frac{1}{2vu^{\frac{3}{2}}} + \frac{1}{v^2 u^{\frac{3}{2}}} - \frac{1}{v^2 \varepsilon r} \right] B(sr) \right. \\ \left. + \varepsilon^4 r^5 \left[\frac{1}{2v^2 u^{\frac{3}{2}}} + \frac{1}{2v^2 (\varepsilon r)^3} + \frac{2}{v^3 u^{\frac{1}{2}}} - \frac{2}{v^3 \varepsilon r} \right] C(sr) \right\} dr$$

where

$$A(sr) = 2J_0(sr) \quad (\text{B3a})$$

$$B(sr) = \frac{2J_0(sr) sr - 2J_1(sr)}{sr} \quad (\text{B3b})$$

$$C(sr) = \frac{2(sr)^3 J_0(sr) - 6J_0(sr)(sr) + 12J_1(sr) - 4J_1(sr)(sr)^2}{(sr)^3} \quad (\text{B3c})$$

The J_0 and J_1 are the zero and first order Bessel functions, respectively. Now we change the variable $\beta = r\tau$. Thus,

$$\begin{aligned}
(20a) &= \frac{1}{R} \{ \bar{v}_1 \sigma_f^2 \lambda \int_0^\tau ds \int_0^\infty \frac{r}{2u^{\frac{3}{2}}} A(sr) dr \\
&\quad + \bar{v}_1 \sigma_f^2 \lambda \int_0^\infty 4 \varepsilon^2 r^3 \left[\frac{1}{2v u^{\frac{3}{2}}} + \frac{1}{v^2 u^{\frac{3}{2}}} - \frac{1}{v^2 \varepsilon r} \right] J_1(\beta) dr \\
&\quad + \bar{v}_1 \sigma_f^2 \lambda \int_0^\infty \varepsilon^4 r^5 \left[\frac{1}{2v^2 u^{\frac{3}{2}}} + \frac{1}{2v^2 (\varepsilon r)^3} + \frac{2}{v^3 u^{\frac{1}{2}}} - \frac{2}{v^3 \varepsilon r} \right] \left[\frac{2J_1(\beta)\beta^2 - 4J_1(\beta) + 2J_0(\beta)\beta}{\beta^2} \right] dr \}
\end{aligned}$$

In above integral one can use the following general integral:

$$\int_0^\tau ds \int_0^\infty \frac{r}{2u^{\frac{3}{2}}} A(sr) dr = \int_0^\infty \frac{\tau J_0(\beta)}{1+r^2+r\sqrt{1+r^2}} dr = 1 - e^{-s} \quad (B4)$$

Finally, (20a) is found as follows:

$$(20a) = \frac{\bar{v}_1}{R} \sigma_f^2 \lambda \left[1 - e^{-\tau} - \varepsilon \int_0^\infty [2rJ_1(\beta) \frac{2u^{\frac{3}{2}} - \varepsilon r(v+2u)}{v^2 u^{\frac{3}{2}}} + F_1(r)] dr \right] \quad (B8)$$

where

$$F_1(r) = \left[\frac{(2 - \beta^2)J_1(\beta) - \beta J_0(\beta)}{r\tau^2} \right] \left[\frac{\varepsilon^3 r^3 (v+4u) + u^{\frac{3}{2}} (5v-4u)}{v^3 u^{\frac{3}{2}}} \right],$$

$$u = 1 + r^2,$$

$$\beta = r\tau,$$

$$v = 1 + r^2 - \varepsilon^2 r^2,$$

Appendix C. Derivation of equation (20c)

Equation (20c) contains the following integral:

$$(20c) = \frac{2\bar{v}_1}{\bar{R}^3} \int_0^t C_{v_1 R} \left(\frac{\bar{v}_1}{\bar{R}} s, 0, 0 \right) ds$$

Here we use equation (17), the cross spectrum between v_1 and R , in order to find $C_{v_1 R}(\xi)$:

$$C_{v_1 R}(\xi) = \frac{\rho_b}{n^2} K^G K_d^G J a \frac{\sinh(\sigma_w)}{\sigma_w} \frac{\sigma_f^2 \mu_1 \mu_2 \mu_3}{\pi^2} \int_{-\infty}^{\infty} \int_{-\infty}^{\infty} \int_{-\infty}^{\infty} \left(1 - \left(\frac{k_1}{k}\right)^2\right)^2 \frac{1}{(1 + (\mu k)^2)^2} \cos(k \cdot \xi) dk$$

Therefore,

$$\begin{aligned} C_{v_1 R} \left(\frac{\bar{v}_1}{\bar{R}} s, 0, 0 \right) &= \frac{\rho_b}{n^2} K^G K_d^G J a \frac{\sinh(\sigma_w)}{\sigma_w} \frac{\sigma_f^2 \mu_1 \mu_2 \mu_3}{\pi^2} \int_{-\infty}^{\infty} \int_{-\infty}^{\infty} \int_{-\infty}^{\infty} \left(1 - \left(\frac{k_1}{k}\right)^2\right)^2 \frac{1}{(1 + (\mu k)^2)^2} \cos(k_1 \frac{\bar{v}_1}{\bar{R}} s) dk \\ &= \frac{\rho_b}{n^2} K^G K_d^G J a \frac{\sinh(\sigma_w)}{\sigma_w} \frac{\sigma_f^2 \mu_1 \mu_2 \mu_3}{\pi^2} \int_{-\infty}^{\infty} \int_{-\infty}^{\infty} \int_{-\infty}^{\infty} \left(\frac{\mu_2^{-2} k_2^2 + \mu_3^{-2} k_3^2}{\mu_1^{-2} k_1^2 + \mu_2^{-2} k_2^2 + \mu_3^{-2} k_3^2} \right)^2 \frac{1}{(1 + k^2)^2} \cos(k_1 \frac{\bar{v}_1}{\mu_1 \bar{R}} s) dk \end{aligned}$$

We change the variable as $s' = \mu_1^{-1} \bar{R}^{-1} \bar{v}_1 s$ and $\tau = \bar{v}_1 t / \mu_1 \bar{R}$ and (20 c) changes to:

$$(20c) = \frac{2}{\bar{R}^2} \frac{\rho_b}{n^2} K^G K_d^G J a \frac{\sinh(\sigma_w)}{\sigma_w} \frac{\sigma_f^2 \mu_1}{\pi^2} \int_0^{\tau} \int_{-\infty}^{\infty} \int_{-\infty}^{\infty} \int_{-\infty}^{\infty} \left(\frac{\mu_2^{-2} k_2^2 + \mu_3^{-2} k_3^2}{\mu_1^{-2} k_1^2 + \mu_2^{-2} k_2^2 + \mu_3^{-2} k_3^2} \right)^2 \frac{1}{(1 + k^2)^2} \cos(k_1 s') dk ds$$

Now we have $\mu_1 = \mu_2 = \lambda$ and $\mu_3 = \varepsilon \lambda$. Thus

$$(20c) = \frac{2}{\bar{R}^2} \frac{\rho_b}{n^2} K^G K_d^G J a \frac{\sinh(\sigma_w)}{\sigma_w} \frac{\sigma_f^2 \mu_1}{\pi^2} \int_0^{\tau} \int_{-\infty}^{\infty} \int_{-\infty}^{\infty} \int_{-\infty}^{\infty} \left(1 - \frac{k_1^2}{k_1^2 + k_2^2 + \varepsilon^{-2} k_3^2}\right)^2 \frac{1}{(1 + k^2)^2} \cos(k_1 s) dk ds$$

Now changing to spherical coordinate system and defining:

$$k_1 = r \cos \beta, k_2 = r \sin \beta, k_3 = k_3$$

$$dk_1 dk_2 dk_3 = r dr d\theta dk_3$$

Therefore we get:

$$(20c) = \frac{2}{R^2} \frac{\rho_b}{n^2} K^G K_d^G J a \frac{\sinh(\sigma_w)}{\sigma_w} \frac{\sigma_f^2 \lambda}{\pi^2} \int_0^\tau ds \int_0^\infty r dr \int_0^{2\pi} d\theta \int_{-\infty}^\infty \left(1 - \frac{r^2 \cos^2 \theta}{r^2 + \varepsilon^{-2} k_3^2}\right) \frac{\cos(sr \cos \theta)}{(1 + r^2 + k_3^2)} dk_3 \quad (C1)$$

In order to derive the integral in equation (C1) we use the general integrals in(B2a) and (B2b).

Furthermore, we use (B3a) and (B3b) along with (B4). The final form of equation (20c) is presented as follows:

$$(20c) = \frac{2}{R^2} \frac{\rho_b}{n^2} K^G K_d^G J a \frac{\sinh(\sigma_w)}{\sigma_w} \sigma_f^2 \lambda \left\{1 - e^{-\tau} + 2\varepsilon^2 \int_0^\infty r^2 \left[\frac{1}{2v u^2} + \frac{1}{v^2 u^{\frac{1}{2}}} - \frac{1}{v^2 \varepsilon r}\right] J_1(\beta) dr\right\} \quad (C2)$$

Appendix D. Derivation of equation (20b)

Equation (20b) contains the following integral:

$$(20b) = \frac{\bar{v}_1^2}{R^2} \int_0^t C_{RR} \left(\frac{\bar{v}_1}{R} s, 0, 0\right) ds$$

$C_{RR}(\xi)$ is as follows(see equation 12):

$$C_{RR}(\xi) = \left(\frac{\rho_b}{n} K_d^G\right)^2 e^{[\sigma_w^2]} (e^{C_{ww}(\xi)} - 1)$$

where

$$C_{ww}(\xi) = \sigma_w^2 e^{-\left|\frac{\xi}{\mu}\right|} = \sigma_w^2 e^{-\sqrt{\left(\frac{\xi_1}{\mu_1}\right)^2 + \left(\frac{\xi_2}{\mu_2}\right)^2 + \left(\frac{\xi_3}{\mu_3}\right)^2}}$$

We consider the mean flow direction along x axis. Thus,

$$C_{ww}(\xi, 0, 0) = \sigma_w^2 e^{-\left|\frac{\xi}{\mu}\right|} = \sigma_w^2 e^{-\frac{\xi}{\mu_1}}$$

We choose $\mu_1 = \lambda$ so that we can calculate (20b) as:

$$(20b) = \frac{\bar{v}_1^2}{R^2} \int_0^t C_{RR}\left(\frac{\bar{v}_1}{R} s, 0, 0\right) ds = \frac{\bar{v}_1^2}{R^2} \left(\frac{\rho_b}{n} K_d^G\right)^2 e^{[\sigma_w^2]} \int_0^t \left(e^{\sigma_w^2 e^{-\frac{\bar{v}_1}{R} s}} - 1\right) ds \quad (D1)$$

Integral in (D1) can be easily derived as explained below. In terms of multimodal porous media the derivation is not straight forward and a numerical integration is performed. In order to derive (D1) for unimodal porous media we use the following singular integrals.

$$Ei(x) = -\int_{-x}^{\infty} \frac{e^{-s}}{s} ds \quad (D2)$$

(D2) is known as exponential integral.

$$Ein(x) = -\int_0^{-x} \frac{1 - e^{-s}}{s} ds = \gamma + \ln(x) + Ei(x) = -\sum_{i=1}^n \frac{x^i}{i \cdot i!} \quad \text{for } x > 0 \quad (D3)$$

(D3) is known as Entire function, and $\gamma = 0.577\dots$ is the Euler's constant. Using the above integrals we can derive the following integral:

$$\begin{aligned}
\int_0^t e^{Ae^{-\alpha\tau}} d\tau &= \sum_{n=0}^{\infty} \int_0^t \frac{A^n e^{-n\alpha\tau}}{n!} d\tau = \sum_{n=1}^{\infty} \frac{1}{-n\alpha} \frac{A^n}{n!} (e^{-n\alpha t} - 1) + t \\
&= -\frac{1}{\alpha} \sum_{n=1}^{\infty} \frac{A^n e^{-n\alpha t}}{n n!} + \frac{1}{\alpha} \sum_{n=1}^{\infty} \frac{A^n}{n n!} + t \\
&= \frac{1}{\alpha} [h(A) - h(Ae^{-\alpha t})] + t \\
&= \frac{1}{\alpha} [Ei(A) - Ei(Ae^{-\alpha t})] \quad (D4)
\end{aligned}$$

Therefore,

$$\int_0^t e^{Ae^{-\alpha\tau}} d\tau = \frac{1}{\alpha} [Ei(A) - Ei(Ae^{-\alpha t})] \quad (D5)$$

Therefore, in case of unimodal distribution of $C_{ww}(\xi)$ the result of (20b) is:

$$(20b) = \frac{\bar{v}_1}{R} \left(\frac{\rho_b}{n} K_d^G \right)^2 e^{[\sigma_w^2]} \lambda [Ei(\sigma_w^2) - Ei(\sigma_w^2 e^{-\frac{\bar{v}}{R\lambda} t})] \quad (D5)$$

References

Allen-King, R.M., Halket, R.M., Gaylord, D.R., Robin, M.J.L.,1998. Characterizing the heterogeneity and correlation of perchloroethene sorption and hydraulic conductivity using a facies-based approach. *Water Resour Res* 34:385–396. doi:10.1029/97wr03496.

Allen-King, R. M., D. P. Divine, M. J. L. Robin, J. R. Alldredge, and D. R. Gaylord, 2006. Spatial distributions of perchloroethylene reactive transport parameters in the Borden Aquifer. *Water Resour. Res.*, 42, W01413, doi:10.1029/2005WR003977.

Bellin, A., A. Rinaldo, W. J. P. Bosma, S. E. A. T. M. van derZee, and Y. Rubin,1993. Linearequilibrium adsorbing solute transport in physically and chemically heterogeneous porous

formations: 1. Analytical solutions. *Water Resour. Res.*, 29(12), 4019–4030, doi:10.1029/93WR02303.

Bellin, A., and A. Rinaldo, 1995. Analytical solutions for transport of linearly adsorbing solutes in heterogeneous formations. *Water Resour. Res.*, 31, 1505–1511.

Bosma, W. J. P., Bellin, A., S. E. A. T. M. van der Zee, & Rinaldo, A., 1993, Linear equilibrium adsorbing solute transport in physically and chemically heterogeneous porous formations: 2. Numerical results. *Water Resour. Res.*, 29(12), 4031–4043, doi:[10.1029/93WR02305](https://doi.org/10.1029/93WR02305).

Bridge, J.S., 2006. Fluvial facies models: Recent developments, in *Facies Models Revisited*, SEPM Spec. Publ., 84, edited by H. W. Posamentier and R. G. Walker, pp. 85–170, Soc. for Sediment. Geol. (SEPM), Tulsa, Okla.

Brusseau, M.L., and R. Srivastava, 1997. Nonideal transport of reactive solutes in heterogeneous porous media: 2. Quantitative analysis of the Borden natural-gradient field experiment. *Journal of Contaminant Hydrology*, 28(2), 115–155.

Cheng, T., Barnett, M.O., Roden, E.E., Zhuang, J., 2007. Reactive transport of uranium (VI) and phosphate in a goethite-coated sand column: an experimental study. *Chemosphere* 68 (7), 1218–1223.

Dagan, G., 1984. Solute transport in heterogeneous porous formations. *J. Fluid Mech.* 145, 151–177.

Dagan, G., 1989. *Flow and Transport in Porous Formations*. Springer Verlag, Berlin.

Dai, Z., Wolfsberg, A., Lu, Z., Deng, H., 2009. Scale dependence of sorption coefficients for contaminant transport in saturated fractured rock. *Geophys. Res. Lett.*, 36, L01403, doi:10.1029/2008GL036516

Dai, Z., Wolfsberg, A.V., Lu, Z., Reimus, P., 2007b. Upscaling matrix diffusion coefficients for heterogeneous fractured rocks. *Geophys. Res. Lett.* 34, L07408, <http://dx.doi.org/10.1029/2007GL029332>.

Dai, Z., Ritzi, R.W., Huang, C., Rubin, Y., Dominic, D.F., 2004. Transport in heterogeneous sediments with multimodal conductivity and hierarchical organization across scales. *J of Hydrology*, 294(1), 68–86.

Dai, Z., Ritzi, R.W., Dominic, D.F., 2005. Improving permeability semivariograms with transition probability models of hierarchical sedimentary architecture derived from outcrop analog studies. *Water Resour Res* 41, W07032, doi:10.1029/2004WR003515.

Davis, J.A., Yabusaki, S.B., Steefel, C.I., Zachara, J.M., Curtis, G.P., Redden, G.D., Criscenti, L.J., Honey, B.D., 2004. Assessing conceptual models for subsurface reactive transport of inorganic contaminants. *Trans. Am. Geophys. Union, EOS* 85(44), November 2.

Deng, H., Dai, Z., Wolfsberg, A., Lu, Z., Ye, M., Reimus, P., 2010. Upscaling of reactive mass transport in fractured rocks with multimodal reactive mineral facies. *Water. Resour. Res.*, 46,W06501. doi:10. 1029/2009WR008363.

Deng, H., Dai, Z., Wolfsberg, A.V., Ye, M., Stauffer, P.H., Lu, Z., Kwicklis, E., 2013, Upscaling retardation factor in hierarchical porous media with multimodal reactive mineral facies. *Chemosphere*, 91(3), 248–257.

Dentz, M., Le Borgne, T., Englert, A., & Bijeljic, B., 2011. Mixing, spreading and reaction in heterogeneous media: A brief review. *Journal of contaminant hydrology*, 120, 1-17.

Fiori, A., Dagan, G., 2002. Transport of a passive scalar in a stratified porous medium. *Transp. Porous Media*, 47, 81–98.

Garabedian, S. P., Gelhar, L. W., Celia, M. A., 1988. Large-scale dispersive transport in aquifers: Field experiments and reactive transport theory Rep. 315Ralph M. Parsons Lab., Dep. of Civ. Eng., Mass. Inst. of Technol., Cambridge.

Gelhar, L.W., 1993. Stochastic Subsurface Hydrology. Prentice-Hall, Englewood Cliffs, NJ.

Gelhar, L.W., Axness, C.L., 1983. Three-dimensional stochastic analysis of macrodispersion in aquifers. *Water Resour. Res.* 19 (1), 161–180.

Gershenzon, N. I., Soltanian, M., Ritzi Jr, R. W., & Dominic, D. F., 2014. Understanding the Impact of Open-Framework Conglomerates on Water-Oil Displacements: Victor Interval of the Ivishak Reservoir, Prudhoe Bay Field, Alaska. arXiv preprint arXiv:1405.3998.

Naum I. Gershenzon, Mohamadreza Soltanian, Robert W. Ritzi & David F. Dominic (2014). Understanding the impact of open-framework conglomerates on water–oil displacements: the Victor interval of the Ivishak Reservoir, Prudhoe Bay Field, Alaska. *Petroleum Geoscience*, DOI: 10.1144/petgeo2014-017

Gershenzon, N. I., Soltanian, M., Ritzi Jr, R. W., & Dominic, D. F., 2014. Influence of small scale heterogeneity on CO₂ trapping processes in deep saline aquifers. arXiv preprint arXiv:1407.0369.

Huang, C., Dai, Z., 2008. Modeling groundwater in multimodal porous media with localized decompositions. *Mathematical geosciences*, 40(6), 689-704.

Lunati, I., Attinger, S., Kinzelbach, W., 2002. Macrodispersivity for transport in arbitrary non-uniform flow fields: asymptotic and preasymptotic results. *Water Resour. Res.* 38 (10). doi:10.1029/2001WR001203.

Miralles-Wilhelm, F., and L. W. Gelhar, 1996. Stochastic analysis of sorption macrokinetics in heterogeneous aquifers. *Water Resour. Res.*, 32(6), 1541–1549, doi:10.1029/96WR00791.

Rajaram, H., 1997. Time and Scale-Dependent Effective Retardation Factors in Heterogeneous Aquifers. *Advances in Water Resources*, 20(4), 217-230.

Rajaram, H., Gelhar, L.W., 1993. Plume-scale dependent dispersion in heterogeneous aquifers: 2. Eulerian analysis and three-dimensional aquifers. *Water Resour. Res.*, 29 (9), 3261–3276.

Ramanathan, R., R. W. Ritzi Jr., and R. M. Allen-King, 2010. Linking hierarchical stratal architecture to plume spreading in a Lagrangian-based transport model: 2. Evaluation using new data from the Borden site. *Water Resour. Res.*, 46, W01510, doi:10.1029/2009WR007810.

Ritzi, R. W. Jr., L. Huang, R. Ramanathan, and R. M. Allen-King, 2013. Horizontal spatial correlation of hydraulic and reactive transport parameters as related to hierarchical sedimentary architecture at the Borden research site. *Water Resour. Res.*, 49, 1901–1913, doi:10.1002/wrcr.20165.

Ritzi, R. W., and R. M. Allen-King, 2007. Why did Sudicky [1986] find an exponential-like spatial correlation structure for hydraulic conductivity at the Borden research site? *Water Resour. Res.*, 43, W01406, doi:10.1029/2006WR004935.

Ritzi, R.W., Dai, Z., Dominic, D.F., Rubin, Y.N., 2004. Spatial correlation of permeability in crossstratified sediment with hierarchical architecture. *Water. Resour. Res.*, 40(3):W03513. doi:10.1029/2003WR002420.

Roberts, P. V., M. N. Goltz and D. M. Mackay, 1986. A Natural Gradient Experiment on Solute Transport in a Sand Aquifer 3. Retardation Estimates and Mass Balances for Organic Solutes. *Water Resources Research*, 22(13), 2047-2058.

Rubin, Y., 2003. *Applied Stochastic Hydrogeology*. Oxford Univ. Press, New York.

Rubin, Y., Sun, A., Maxwell, R., and Bellin, A. , 1999. The concept of block-effective macrodispersivity and a unified approach for grid-scale-and plume-scale-dependent transport. *Journal of Fluid Mechanics*, 395, 161-180.

Samper, J., Yang, C., 2006. Stochastic analysis of transport and multicomponent competitive monovalent cation exchange in aquifers, *Geosphere* 2 (2), 102-112.

Soltanian, M.R., Ritzi, R.W., Dai, Z., Huang, C.C., Dominic, D., 2014, Transport of kinetically sorbing solutes in heterogeneous sediments with multimodal conductivity and hierarchical organization across scales, *Stoch. Environ. Res. Risk. Assess*, doi:10.1007/s00477-014-0922-3

Soltanian, M.R., Ritzi, R.W., 2014, A new method for analysis of variance of the hydraulic and reactive attributes of aquifers as linked to hierarchical and multiscaled sedimentary architecture, *Water Resources Research*, doi: 10.1002/2014WR015468

Whitaker, S., 1999. *The Method of Volume Averaging*. Kluwer Academic Publishers.

Yang, C., Samper, J., 2009. Numerical evaluation of multicomponent cation exchange reactive transport in physically and geochemically heterogeneous porous media, *Computational Geosciences*, 13 (3), 391-404

Zavarin, M., S. F. Carle, and R. M. Maxwell, 2004), *Upscaling Radionuclide Retardation-Linking the Surface Complexation and Ion Exchange Mechanistic Approach to a Linear Kd Approach*, UCRL-TR-204713, Lawrence Livermore National Laboratory, Livermore, California.

Zhang, Y., Green, C.T., and Fogg, G.E., 2013. The impact of medium architecture of alluvial settings on non-Fickian transport. *Advances in Water Resources*, 54: 78–99, doi: 10.1016/j.advwatres.2013.01.004.

Zhang, Q., 1998. Multi-length-scale theories for scale-up problem and renormalized perturbation expansion. *Adv. Water Res.* 20, 317–333.

Zhou, Y., Ritzi, R.W., Soltanian, M. R., and Dominic, D. F., 2014. The Influence of Streambed Heterogeneity on Hyporheic Flow in Gravelly Rivers. *Groundwater*, 52(2), 206-216.